

PCCP

Accepted Manuscript



This is an *Accepted Manuscript*, which has been through the Royal Society of Chemistry peer review process and has been accepted for publication.

Accepted Manuscripts are published online shortly after acceptance, before technical editing, formatting and proof reading. Using this free service, authors can make their results available to the community, in citable form, before we publish the edited article. We will replace this *Accepted Manuscript* with the edited and formatted *Advance Article* as soon as it is available.

You can find more information about *Accepted Manuscripts* in the [Information for Authors](#).

Please note that technical editing may introduce minor changes to the text and/or graphics, which may alter content. The journal's standard [Terms & Conditions](#) and the [Ethical guidelines](#) still apply. In no event shall the Royal Society of Chemistry be held responsible for any errors or omissions in this *Accepted Manuscript* or any consequences arising from the use of any information it contains.



Journal Name

ARTICLE

Time-dependent quantum simulation of coronene photoemission spectra

Received 00th January 20xx,
Accepted 00th January 20xx

Angela Acocella^a, Monica de Simone^b, Fabrizio Evangelista^c, Marcello Coreno^d, Petra Rudolf^c and Francesco Zerbetto^a

DOI: 10.1039/x0xx00000x

www.rsc.org/

Photoelectron spectroscopy is usually described by a simple equation that relates the binding energy of the photoemitted electron, E_{binding} , its kinetic energy, E_{kinetic} , the energy of the ionizing photon, E_{photon} , and the work function of the spectrometer, Φ , $E_{\text{binding}} = E_{\text{photon}} - E_{\text{kinetic}} - \Phi$. Behind this equation there is an extremely rich physics, which we describe here using as an example a relatively simple conjugated molecule, namely coronene. The theoretical analysis of valence band and C1s core level photoemission spectra showed that multiple excitations play an important role in determining intensities of the final spectrum. An explicit, time-evolving model is applied, able to count for all possible photo-excitations occurring during the photoemission process, showing they evolve on a short time-scale, of about 10 fs. The method reveals itself to be a valid approach to reproduce photoemission spectra for Polycyclic Aromatic Hydrocarbons (PAHs).

Introduction

Photoelectron spectroscopy (PES) monitors the energy of electrons emitted from solids, gases, or liquids by the photoelectric effect. Depending on the source of ionization energy, PES can be divided into Ultraviolet Photoelectron Spectroscopy (UPS) and X-ray Photoelectron Spectroscopy (XPS) that probe either valence or core electrons. Photoelectron spectroscopy of core levels is a quantitative spectroscopic technique that is often used for determining the elemental composition of a solid or liquid surface¹ or to retrieve information on chemical environments or oxidation states of the atoms present in a gas, liquid or solid.² Valence band photoemission features of molecules in the gas phase can be related to the different molecular orbitals, while those of an adsorbate on a solid surface reveal whether physisorption or chemisorption has taken place. The spectra are obtained by irradiating a material with a monochromatic beam of photons and, subsequently, measuring the number of electrons that escape from the sample as a function of their kinetic energy (E_{kinetic}). PES can measure the energies of the ground and excited states, after the loss of an electron from a neutral system. Indeed, since the energy of the photon is known, one can determine the electron binding energy of the emitted electrons as:

$$E_{\text{binding}} = E_{\text{photon}} - E_{\text{kinetic}} - \phi \quad 1.$$

where, E_{binding} is the energy difference between the initial and the final state corresponding to the situations before and after the photoemission event has taken place, E_{photon} is the energy of the photons, E_{kinetic} is the kinetic energy of the emitted electron, and Φ is the work function of the spectrometer (not the material).

Despite the deceiving simplicity of eq. 1, the physics of photoelectron spectroscopy is extremely rich and the interpretation of its spectra is not straightforward. The high energy of the photon triggers a complicated re-organization of the wavefunction where the usually dominant one-photon contribution of equation 1 is combined with all other possible contributions of the same energy, together with the continuum states of the ionized system. In short, the final ionized state is non-stationary and is a time-evolving wavepacket whose investigation requires time-dependent calculations.

Ionization processes in atoms and molecules induced by strong fields have been described with different methods that allow to calculate resonance states activated in non-linear phenomena. The single-active electron approximation for numerical integrations of the Time Dependent Schrödinger Equation, TDSE, may accurately describe some aspects of strong-field atomic ionization, as demonstrated by Muller et al.³⁻⁵ Thachuk, Ivanov and Wardlaw have employed the TDSE to propagate the electrons and classical dynamics for the nuclei to simulate above threshold ionization, ATI, and dissociation in H_2^+ and HCl molecules,^{6,7} while, Bandrauk et al. used accurate numerical integrations of wavepackets to study

^a Dipartimento di Chimica "G. Ciamician", Università di Bologna, V. F. Selmi 2, I-40126 Bologna, Italy

^b CNR-IOM Lab TASC, ss. 14 km 163,5, Basovizza, I-34149 Trieste, Italy.

^c Zernike Institute for Advanced Materials, University of Groningen, Nijenborgh 4, NL-9747AG Groningen, The Netherlands

^d CNR-ISM, uos Trieste, ss.14 km 163,5 Basovizza, I-34139 Trieste, Italy

the full quantum dynamics of H_2^+ and H_2 in intense laser fields,⁸⁻¹⁹ providing insight into the laser-induced ionization and dissociation process, and explaining multi-photon phenomena such as ATI and high-order harmonic generation. The complex scaling method²⁰ rotates the coordinates into the complex plane, although it is difficult to apply it in time-dependent calculations. The variational method,^{21,22} and least-squares schemes²³ have also been introduced in the calculation of continuum wave functions, but efficient and accurate solutions are still necessary.

Here, we propose a time-dependent quantum mechanical method to assign and interpret photoelectron spectra of large conjugated systems, in particular PAHs (Polycyclic Aromatic Hydrocarbons), by studying the onset of the ionization dynamics activated by the excitation process with explicit wavepacket dynamics calculations. The proposed method provides a way to directly correlate the time-dependent wavefunction recombination to intensities of photoelectron spectra.

The ionization spectra of PAHs have received large attention over the last decades: there is evidence of their substantial presence in interstellar carbon and ices, and it is also known they are carriers of interstellar IR absorption and emission bands in a wide variety of sources.^{24,25} Regarding our daily life, PAHs have been demonstrated to show mutagenic and carcinogenic activities,²⁶ as well as to be produced in combustion processes of organic compounds.²⁷ They can also be employed as building blocks of efficient electronic devices.^{28,29} The investigation of their electronic structure and the interpretation of their spectra has been widely advocated. Here, we test the accuracy and efficiency of an in-house developed method on the simulation of coronene valence and core photoelectron spectra. Their successful interpretation can open the way to the analysis of ionization spectra for other larger PAHs molecules, assisting the understanding of chemical reactions they are involved in.

The coronene ultraviolet photoelectron spectrum is characterized by sharp, well-separated peaks of roughly similar intensities below ~ 10 eV. They are interpreted in terms of Koopmans' theorem as π -electron ionization peaks and have only little or no vibrational structure. In the higher energy region, on the contrary, these sharp features start to overlap broad structures, identified as the σ ionization manifold. Both the π - and σ -band features are spread and overlap with shake-up satellites structures, a mixture of excited state configurations. The loss of an electron from a σ orbital weakens a chemical bond significantly, tends to make the σ and the π orbitals indistinct from one another, and produces a dense manifold of vibrational progressions that accompanies the ionization peak. The intricacy of the spectral features makes it necessary to resort to simulations to analyse experimental measurements at bonding energies larger than 10 eV. The simulation of a photoelectron spectrum requires sophisticated quantum chemical models with a strong quantum mechanical basis.³⁰⁻³⁸

The valence band photoemission spectrum of coronene has been investigated by approaches based on the Green Function,

GF, formalism.³⁷ The accuracy of the prediction was about 0.3 eV, with a sensitivity to the details of calculations, mainly the basis set, that decreased with increasing binding energy. The author identified as a reason for the trend the fact that, for the outermost levels, the leading second-order corrections to orbital binding energies are pair-removal corrections, which arise from the particle component of the self-energy and imply double electronic excitations, while at higher binding energies the dominating terms are orbital and pair relaxation terms linked to the hole component of the second-order self-energy. One of the drawbacks of the Green Function calculations was the systematic underestimation of the ionization threshold, which implies that the excitation energies in the cation are systematically overestimated. A different approach, namely Time Dependent Density Functional Theory, TDDFT, circumvents this difficulty, by ascribing the ionization thresholds of the neutral molecules to the zero of excitation energies in the cations, while it is less accurate for other aspects.³⁹⁻⁴² Overall, the computational approaches to the spectra of coronene have been quite successful and the limitations of the computational models have been well outlined.³⁷

Recently, time-resolved photoelectron spectroscopy has been employed to study ultrafast non-adiabatic processes on neutral polyatomic molecules, taking into account both electronic and vibrational contributions.⁴³ In short, it is fair to summarize the results by saying that the complicated picture of coronene valence band photoemission means that the phenomenon cannot be described as the simple ionization of a binding electron.

Experimental Section

The photoemission spectra were taken at the Gas Phase Photoemission beamline at the Elettra synchrotron in Trieste, Italy, using a 6-channel, 150 mm hemispherical electron energy analyzer. The electron analyzer was mounted in the plane defined by the (linearly polarized) electric vector of the light and the photon propagation direction at an angle of 54.7° with respect to the electric vector of the light. In this geometry the axis of the analyzer is set at the pseudo magic angle, and so measurements should be insensitive to the photoelectron asymmetry parameter β .

Coronene crystalline powder (Sigma-Aldrich, minimum purity of 99%) was used without any further purification and sublimed from a homebuilt furnace⁴⁴ at $T \sim 478$ K. Sample purity was checked by comparing with the valence band photoemission spectra recorded during progressive heating, until we obtained a spectrum comparable to those available in the literature.⁴⁵ This comparison also assured that the sample did not suffer from thermal degradation or radiation damage. The valence band photoemission spectrum, showed in Figure 1(a), was recorded at 21.50 eV, with an overall energy resolution better than 100 meV; these improved experimental conditions in terms of overall flux and resolution allowed

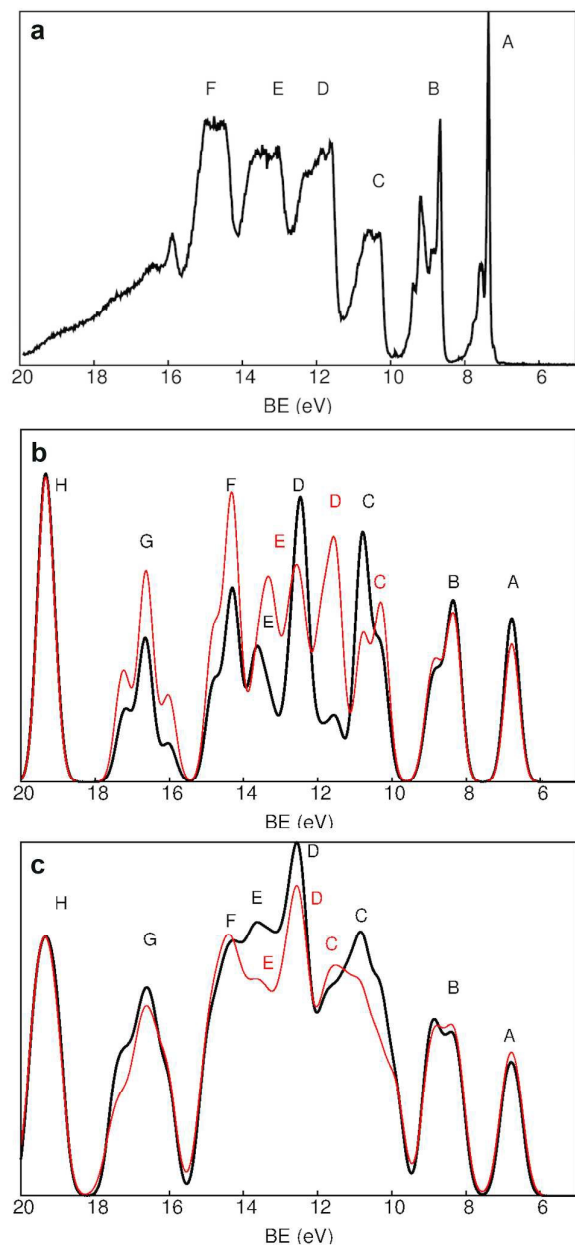


Figure 1. (a) Experimental valence photoemission spectrum of coronene. Peaks are labelled from A to F; (b) CAM-B3LYP/CCPVDZ convoluted valence photoemission spectrum of coronene at 0 K, calculations were carried out with a constant (red line) and ramped up and down (black line) field envelope. Peaks are labelled from A to H in black colour. Where band positions differ, labels are indicated in red for the constant envelope; (c) CAM-B3LYP/CCPVDZ convoluted valence photoemission spectrum of coronene statistical ensemble, colour code as in (b).

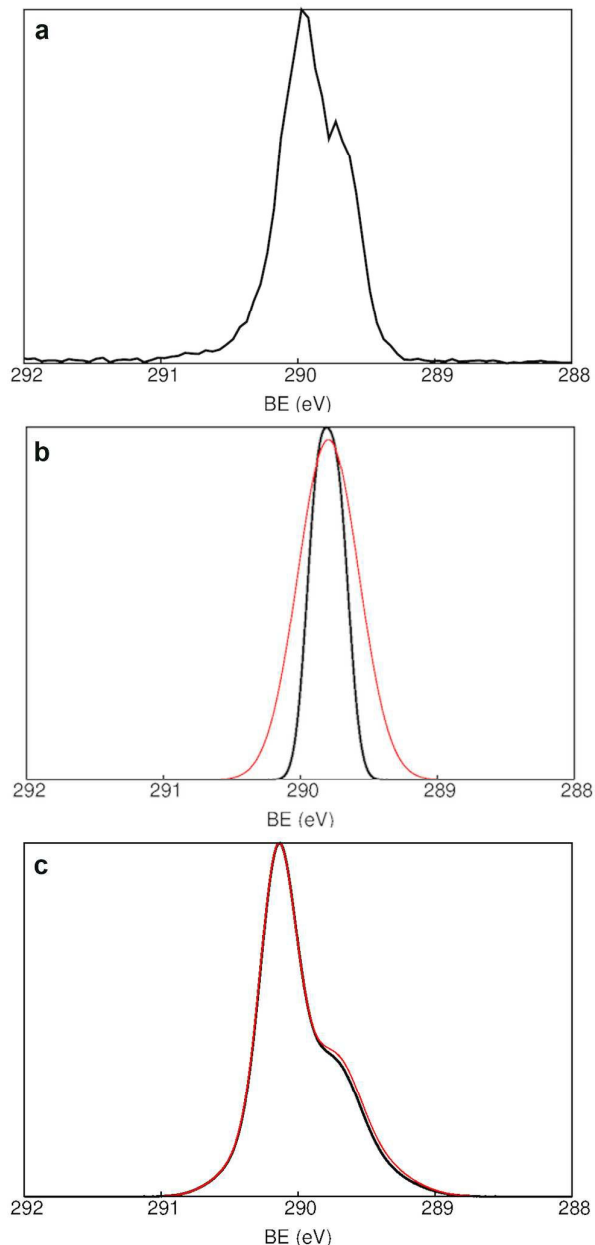


Figure 2. (a) Experimental C1s core level photoemission spectrum of coronene; see ref. 38; (b) CAM-B3LYP/CCPVDZ convoluted C1s core level photoemission spectrum of coronene at 0 K, calculations were carried out with a constant (red line) and ramped up and down (black line) field envelope; (c) CAM-B3LYP/CCPVDZ convoluted C1s core level photoemission spectrum of coronene statistical ensemble, colour code as in (b).

ionisation of electronic states in the inner valence region and a better resolution of the vibrational envelope of the peaks below 10 eV of ionization energy.

The carbon 1s core level photoelectron spectrum, displayed in Figure 2(a), was recorded at photon energy of 350 eV, with an overall experimental resolution of 250 meV.

Details of the 1s core experimental setup and its recording have been described in Ref 38.

The theoretical basis

The photoelectron process can be described as the transition of one electron from an initial occupied state to a final empty free-electron level in vacuum. In a molecule, the final state corresponds to the final state of an optical excitation: initially in the unperturbed state $|i\rangle$, the molecule absorbs one photon, reaching the final state $|f\rangle$. If we assume that all virtual (empty) orbitals share the same probability of losing the electron to the continuum of levels of the vacuum, we can approximate the photoemission to a process similar to an optical absorption. The initial stationary state $|i\rangle$, here $\Psi(0)$, i.e., $\Psi(t=0)$ in Eq. 2, is the initial electronic wavefunction of the system in the absence of external perturbation.

The interaction of $\Psi(0)$ with an external electric field produces a non-stationary state. The time evolution of the wavefunction in the presence of an external perturbation can be carried out with the stable propagator algorithm proposed by Allen and co-workers,⁴⁶⁻⁴⁹ that reads:

$$\Psi(t + \Delta t) = \left(\frac{1 + i\hat{H}\Delta t}{2\hbar} \right)^{-1} \left(\frac{1 - i\hat{H}\Delta t}{2\hbar} \right) \Psi(t) \quad 2.$$

where, $\Psi(t)$ is a wavepacket; Δt is the time step; \hat{H} is the total Hamiltonian, given by the sum of the unperturbed molecular Hamiltonian, \hat{H}^0 , and the perturbing Hamiltonian, $\hat{H}(t)$. This latter represents the interaction between the classical electric field and the molecular dipole moment, here written as:

$$\hat{H}(t) = -\hat{D}\varepsilon(t)\sin(\omega t) \quad 3.$$

where, $\hat{H}(t)$ is the product of the matrix of the dipole moments between atomic orbitals, \hat{D} , and the sinusoidal wave of the oscillating external field; ω is the frequency of the incoming photon; $\varepsilon(t)$ is the electric field amplitude or field envelope. The field envelope is either kept constant in time, or ramped up and down during the dynamics. The calculations are carried out in the atomic orbital framework. The field polarization can be chosen. The coefficients of $\Psi(t)$ are updated at each time step under the effect of the external field. The propagation is carried out starting from molecular orbitals orthonormalized by the Löwdin transformation.

The approach has been successfully employed by us also to investigate the photolytic splitting of water ice by VUV light,⁵⁰ the dynamics of photo-activated chemical bonding,⁵¹ electron transfer processes⁵², photo-induced dissociation,⁵³ non linear optical properties,⁵⁴ and mono- and multi-photon excitations.⁵⁵

The evolution of the electronic wavefunction is therefore calculated with a generalized Cayley algorithm, based on a Dyson-like expansion of the time-evolution operator,⁵⁶ which conserves probability and preserves orthogonality. Being intrinsically an $O(N)$ method once the initial state has been specified, it is well-suited to investigate large systems, such as complex materials and biological molecules, as also shown by our previous applications. Numerically, the time-dependent Schrödinger equation is solved by the Crank-Nicolson approximation method,^{57,58} based on expressing the exponential operator $\exp(H\Delta t)$ with second-order accuracy. It is the commonly recommended finite differences scheme to approximate the solutions of the TDSE in complex multiscale phenomena. It is a stable approach, which assures the normalization to unity of the wave function independently of the time step size Δt . In contrast, the accuracy of the calculated solution obviously depends on time step parameter: being the method second order in time, the accuracy increases by a factor of four if the step size is halved. This kind of simulations always requires a compromise between running time and accuracy of the solution. In our case, a time step of 0.0096 fs and a simulation length of 1024 total steps ensure a suitable accuracy of the solution.

There are a number of other methods usually used in numerical solutions that can be robust propagators for general time-dependent applications, including i) the general split-operator methods (SOM),^{59,60} ii) the efficient large-vector-matrix operations,^{61,62} iii) the Chebyshev Polynomial method⁶³ and iv) the iterative Lanczos method⁶⁴. Additionally, when the initial state is the ground state, the TDSE can be propagated for an arbitrary initial vector using the imaginary-time-propagation, ITP, method⁶⁵, which is quite efficient if only part of the eigenstates is needed.

In our model, the presence of the electric field polarizes the wavefunction and induces transitions between the states of the system that can be described, at every time, by a transition current probability (or electron flux)^{66,67}, a gauge invariant, origin-independent vector field, expressed as:

$$J_{ij} = \frac{1}{2m} \left(\Psi_i \hat{p}^* \Psi_j^* + \Psi_i^* \hat{p} \Psi_j \right) \quad 4.$$

where, Ψ_i is the time-evolving wavefunction of the state from where the transition initiates; \hat{p} is the matrix of linear momentum operator; Ψ_j is the wavefunction of the state where the transition ends; J_{ij} is the electron flow of probability across orbitals in time, a valuable tool to investigate magnitude and direction of the electronic motions in our context.

By assuming that during the simulation time of a single electron dynamic (up to 10.0 fs) the nuclei do not move substantially, we can say that the photoelectron spectrum, $P(E, t)$, at a fixed energy E and time t , is directly proportional to the electric transition dipole moment⁶⁸, D_{ij} , which is, in turn, related to the transition current density between the i th

and j th non-stationary state, in the configuration space representation, throughout the following relation:⁶⁹

$$J_{ij} = \frac{\epsilon_j - \epsilon_i}{i\hbar} D_{ij} \quad 5.$$

where, ϵ_i and ϵ_j are the energies of the involved states.

Being the photoelectron spectrum a coherent superposition of amplitudes of ionization processes at different times, the time integration of the electron flux over the total simulation length returns a photoelectron spectral profile, whose intensities are proportional to those of the experimental spectrum. The calculation of the density current probability between all molecular orbitals induced by the external perturbation can thus provide a direct description of the photoelectron process under the above assumptions.

As a guide to the eye, the calculated stick peaks of the density current contributions are convoluted with Gaussian functions. Nuclei are frozen during the simulations. Therefore, in the effort to capture the experimental conditions and to account for the Jahn-Teller distortions, expected for degenerate energy levels in conjugated molecules, a zero-point energy sampling of coronene molecules are produced via the BOMD^{70,71} routine implemented in the Gaussian09 suite of programs.⁷² Thermal energy distortion is added to the D_{6h} geometry.^{70,73-75} Room temperature and vibrational normal modes are used to generate a statistical number of structures (namely, 384, a purely randomly generated number). This procedure provides a statistical ensemble of geometries identical in energy, but different in their vibrational energy distribution about the equilibrium geometry, allowing taking into account vibrationally induced distortions. The photoelectron spectra calculated for the ensemble of thermally equilibrated coronene structures include vibrational effects, overcoming some limitations of the method.

The vertical ionization energy is calculated according to the IP theorem,⁷⁶⁻⁷⁹ that states that the energy of the highest occupied molecular orbital (HOMO) equals the negative of the gas-phase molecular ionization potentials (IP). Binding energies of the entire photoelectron spectrum are then assigned according to the DFT Koopmans' theorem. Therefore, the choice of the appropriate functional is crucial for the reproduction of experimental ionization spectra. Unfortunately, the Kohn-Sham eigenvalues obtained through the use of the general LDA or GGA approximations are often not in good agreement with experiments:⁸⁰ the IP theorem is grossly violated, and the negative of the HOMO energy usually underestimates the IP severely.⁸¹⁻⁸⁴ The calculated eigenvalue spectrum may still exhibit qualitative failure even by rigidly shifting the theoretical energies,^{85,86} because of a wrong ordering of the molecular orbitals.

The situation can be improved using "hybrid" DFT functionals,⁸⁷ but, even in these cases, the HOMO energies, although closer to experimental ionization energies, significantly underestimate those observables (as shown by our B3LYP calculations on the coronene molecule, mentioned below in the text). The main reason for the failure resides in

the difficulty to obtain the correct $1/r$ asymptotic potential that is "experienced" by an electron at large distances from the molecule, which is relevant for describing the ionization process.

A promising strategy for overcoming such problem is offered by the more recent class of range-separated hybrid (RSH) DFT functionals, pioneered by Savin and co-workers.⁸⁸ In these functionals, the Coulomb repulsion term is separated into long-range (LR) and short-range (SR) components, via a range-separation parameter, γ . The LR term, mapped using full Fock exchange, establishes the correct asymptotic potential.

In our simulations, we show that, not only the IP, but also the entire valence-electron spectrum of the coronene molecule can be accurately described by the eigenvalues of a RSH functional, namely the CAM-B3LYP, introduced by Yanai et al.⁸⁹ and based on the Coulomb-attenuating method (CAM). The approximation follows original work of Hirao and coworkers^{90,91} and Savin and coworkers.^{88,92} Preliminary investigations⁸⁹⁻⁹⁷ have demonstrated that CAM-B3LYP provides significantly improved Rydberg and charge transfer (CT) electronic excitation energies, due to an enhanced description of the long-range exchange interaction. For extended π -conjugated systems, where DFT calculations give highly inaccurate results, it has been demonstrated that range-separated density functionals including variable fractions of orbital exchange,^{98,99} such as CAM-B3LYP, LC- ω PBE, and ω B97X, provide good accuracy.¹⁰⁰⁻¹⁰²

A recent work on the calculation of the water monomer photoelectron spectra proved that the CAM-B3LYP results are quantitatively close to the experiment.¹⁰³ Moreover, the photoelectron spectrum of N-heterocyclic carbenes (NHCs) was recently studied with the long-range corrected CAM-B3LYP functional, showing how the approach provides satisfactory agreement for the low-lying (i.e. single excitations-dominated) transitions. The agreement is not inferior to that of the other methods used for calculating the monopole-allowed direct shake-up transitions.¹⁰⁴

A further improvement of results can be obtained by using optimally tuned RSH (OT-RSH) functionals⁹⁸ where the parameter γ is tuned for each kind of system, or some modeled exchange potential that has correct asymptotic behavior, such as the Leeuwen and Baerends potential¹⁰⁵, which will be considered in future calculations.

The ground electronic state of coronene was then calculated with Gaussian09⁷², at the CAM-B3LYP/CCPVDZ level of calculations (using Dunning's correlation-consistent polarized valence basis set of double- ξ quality level).^{89,106}

The perturbing field was applied perpendicularly to the plane of the molecule. Photon frequencies, ω , corresponding to energies of 21.50 eV and 350 eV, were used to reproduce experimental valence and C1s core photoelectron spectra, respectively. Two sets of electron dynamics for the cooled geometry and for the ensemble of coronene molecules were run to calculate the corresponding valence and C1s photoelectron spectra. In the first set, the field strength was kept constant during the simulation time, at a fixed value of 0.1 au. In the second one, it was ramped up and down:

initially, in the first 3 fs, it was linearly increased to the maximum value, ϵ_{max} , of 0.1 au, it was then left constant at ϵ_{max} for 3 fs, and then linearly decreased to zero in the last 3 fs of the simulations. The total pulse duration in the varying envelope simulations corresponds to 16 and 255 optical cycles for frequencies field of 27.50 eV ($\tau = 190$ as) and 350 eV ($\tau = 11.7$ as), respectively. In both field envelope settings, the total time duration of the field source is about 10.0 fs.

Computationally, the high intensity corresponds to the field experienced by the molecule when the photon is impinging on it. Schlegel et al. indicated field strengths of about $1.72 \cdot 10^{14}$ W/cm² to simulate ionization in H₂⁺.¹⁰⁷ Usually, for atoms and diatomic molecules in high-intense field regimes, the Keldysh parameter¹⁰⁸, γ , is used to distinguish, for a given electric field and a laser frequency, if the ionization is mediated by the absorption of a photon, or by the electric field of the laser. In particular, $\gamma \gg 1$ indicates a multi-photon ionization regime, $\gamma \approx 1$ corresponds to the tunneling regime, and $\gamma \ll 1$ to the over the barrier ionization. The Keldysh parameter is calculated, in atomic units, as:

$$\gamma = \sqrt{\frac{|I_p|}{2U_p}} \quad \text{and} \quad U_p = \frac{F_0^2}{2\omega^2} \quad 6.$$

where, I_p is the ionization potential, U_p is the ponderomotive potential and F_0 and ω are the amplitude and angular frequency of the laser field, respectively.

The Keldysh parameter is used here as a reference quantity to assign the ionization mechanism, even though it was shown, with a numerical model assuming a one-dimensional potential, that its value is strongly structure dependent and that large molecules reach the field ionization region already at $\gamma > 1$.¹⁰⁹ For large systems, the quasi-static and single active electron, SAE, approximations are believed to breakdown and ionization is controlled by either an adiabatic or a non-adiabatic multi-electron, NME, process, where the wavelength dependence of the photoionization rate may be much different than the classical prediction.¹¹⁰⁻¹¹²

Experiments on large molecules like ethene, propane, propyne, benzene, toluene and methanol^{113,114} and long chain molecules, hexatriene, decatetraene and β -carotene suggest a screening effect of the electric field due to the large extent of the delocalized electrons and consequently a decreased probability for field ionization¹¹⁵. In our simulations, with a field intensity of $3.5 \cdot 10^{14}$ W/cm², Keldysh parameters are 7.39 and 5.87 for the valence photoelectron and C1s processes, respectively. In both cases, we can say that our calculations are in the multi-photon ionization regimes.

Results

The past computational analysis of the photoelectron spectra of coronene showed the important role played by multiple excitations. In the model used here, these excitations appear

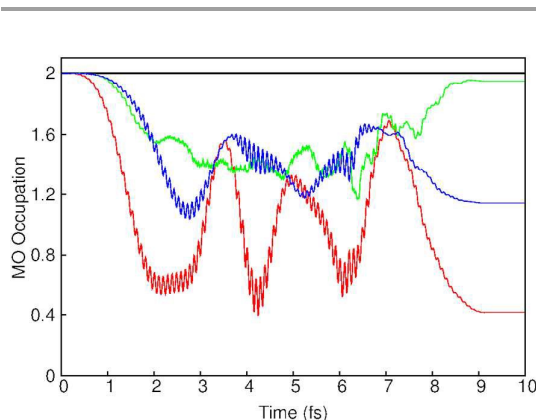


Figure 3. Time evolution of four coronene molecular orbitals under the effect of an electric field with a field frequency of 21.5 eV, and a variable envelope, ramped up and down as described in the text above. Lowest energy core orbital solid black line at the top of the Figure; HOMO, red solid line; lowest valence orbital, green solid line; valence orbital in resonance with the field frequency, blue solid line.

directly, as shown in previous work, where multi-photon transitions and non-linear optical properties were obtained.⁵⁴ The electron dynamics re-arranges the wavefunction and populates orbitals that in the absence of the electric field are unoccupied. The electron can then backscatter to orbitals that were initially occupied but have become unoccupied in the course of the dynamics. Therefore, shake-up states are included in this theoretical approach, although their energies are positioned at binding energies of the initial unperturbed wavefunction.

The simulations at the CAM-B3LYP/CCPVDZ level were run on the initial eigenfunctions of the unperturbed molecular Hamiltonian for a few femtoseconds (up to ~ 10.0 fs). The length of the dynamics was determined in the constant field envelope simulation by the time required by the wavefunction to reach the minimum of the electron occupation, which should correspond to the maximum in the probability of ionization.

A typical dynamics: As an illustration, Figure 3 shows a typical time evolution of the occupation of four key molecular orbitals of planar coronene during the simulation of the valence band photoemission for the CAM-B3LYP/CCPVDZ case. The perturbation is an oscillating electric field with an envelope ramped up and down, as described above, to a maximum value of ϵ_{max} at 0.1 au and a field frequency of 21.5 eV. The occupation of the lowest-energy core orbital, characterized by an unperturbed energy of about 280 eV, remains stationary during the entire evolution (solid black line at the top of Figure 3), because of the large mismatch with the photon energy, meaning that the latter is far too low to perturb it. The occupation of other molecular orbitals that are displayed, namely, the HOMO (Highest Occupied Molecular Orbital), the

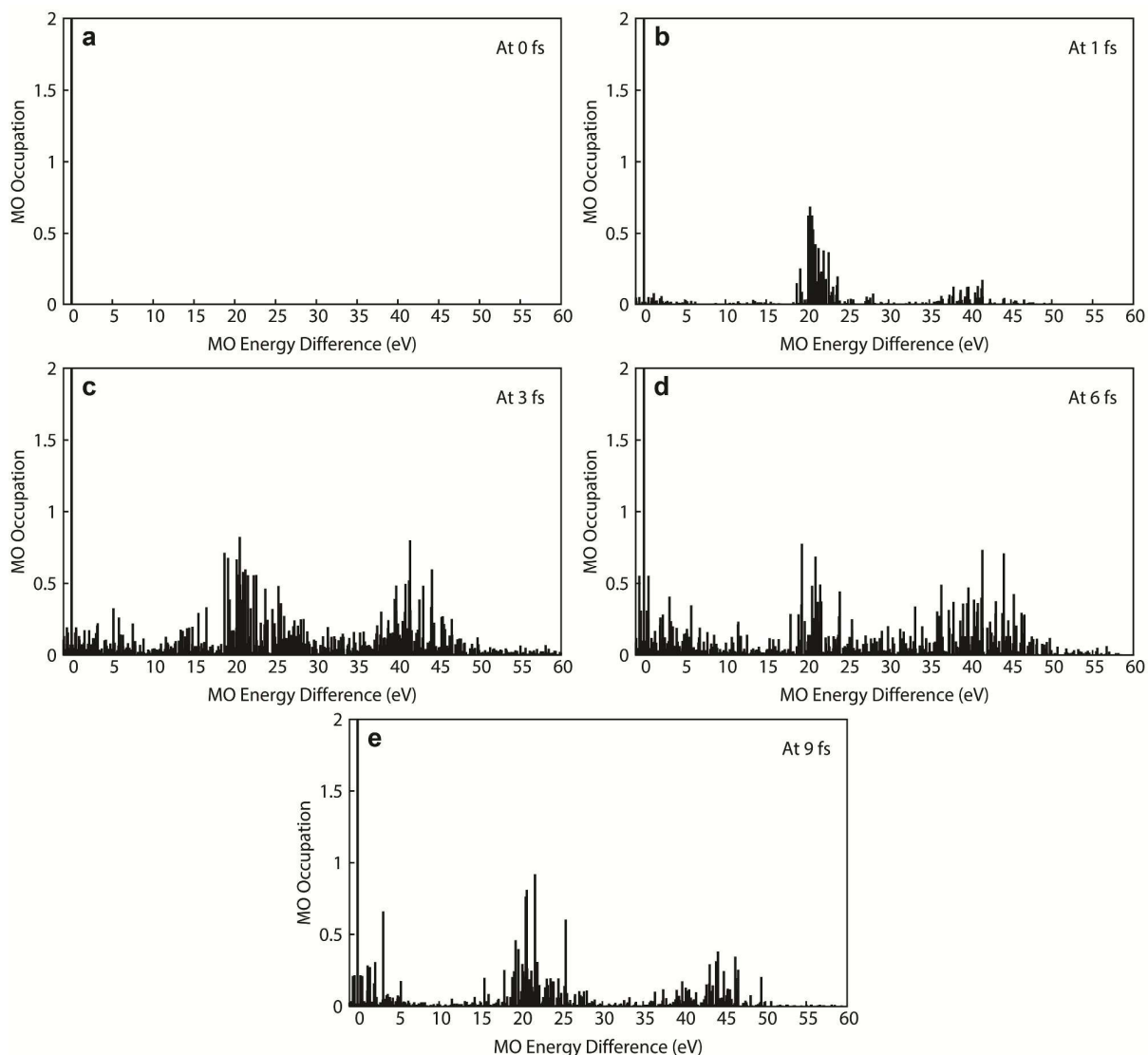


Figure 4. The electron density matrix in the molecular orbital basis, ρ_{ij} , calculated as a function of the MO's energy difference at **a)** 0 fs, **b)** 1 fs, **c)** 3 fs, **d)** 6 fs and **e)** 9 fs of the simulation.

lowest valence orbital, characterized by an unperturbed energy of nearly 27 eV, and the valence orbital with an unperturbed energy on resonance with the field frequency, 21.5 eV, decrease differently during the simulation, and oscillate with characteristic frequencies corresponding, to a good approximation, to Rabi frequencies calculated according to equation 26 in reference 107.

The electron density matrix in the molecular orbital basis, ρ_{ij} , is also calculated as a function of the MO's energy difference at 0, 1, 3, 6 and 9 fs of the simulation, in order to display how the coherent superposition of inner molecular orbitals takes place

during the simulation. The time-dependent matrix elements, $\rho_{ij}(t)$, change due to the electric field. The diagonal matrix elements represent the MO electron occupancy associated to the i -th molecular orbital; the off-diagonal ones are the electron occupancy due to the "migration" from the i -th to j -th MO.

As Figure 4 shows, the electron density mainly flows between those orbitals whose energy difference is ~ 21.5 eV and ~ 43 eV, i.e., corresponding to one- and two-photon transitions. The initially unoccupied orbitals become successively occupied according to their increasing energy and the main populated

orbitals are those in resonance with the field frequency (or its multiples). The higher excitation requires longer times or stronger fields to occur. By comparing figures 4a to 4e, it is possible to assess the coherence of the process. A measure of such a coherence can be the spread of the excitation. The initially coherent states spread and lose coherence until the field is switched off.

The calculated spectra: Figures 1(b) and 2(b) show the valence and the C1s photoemission spectrum, respectively, calculated for the “cooled” coronene geometry, at the CAM-B3LYP/CCPVDZ level, together with the comparison between the two different field envelope settings (vide supra).

The peaks are broadened with a Gaussian function characterized by a FWHM of 0.2 eV. Figures 1(c) and 2(c) display the valence and the C1s photoemission spectrum, respectively, calculated for the thermally equilibrated coronene ensemble, together with a comparison between the two different settings of the field envelope. Again, stick spectra are broadened with a Gaussian function, whose FWHM, for both Figures 1(c) and 2(c), is calculated as the standard deviation over all molecular orbital energies of different structures. In particular, photoemission spectra obtained with constant field strength of 0.1 au are displayed with a red solid line, while those calculated with a ramped up and down field envelope, with a black solid line. The main bands of UPS spectra were labelled from (A) to (H) in black colour. To assist the eye, where band positions differ, labels are (also) indicated with red colour for the constant field strength. Binding energies are always given in eV. Calculated spectra are compared with the corresponding experimental spectra showed in Figure 1(a) and 2(a). As the comparison shows, the differences between the results of the two field envelopes concerns the σ -band system in the region between 10 and 14 eV, where positions and relative intensities of bands from C to E are (slightly) modified, especially for the cooled coronene system. All other bands are not greatly affected by the modification of the field envelope. The variation of the spectrum in the σ -region, although not pronounced, was not unexpected, considering the complexity of the ionization bands, with many and severely overlapping ionization lines at binding energies larger than 10 eV. C1s spectra do not show substantial differences between the two field envelope sets.

The electron dynamics: The agreement of the calculations with the valence and core level photoemission spectra suggests that the model is accurate and justifies a deeper investigation of the results of the calculations. We examined the largest contributions to the fluxes, or current densities, which govern the band intensities. A weaker field decreases the flux and the associated probability of ionization (not shown). The Fourier transform of the fluxes provided a variety of very rapid frequencies that could not be correlated to individual orbital energies or specific transition energies.

In equation 1, the transition starts from an occupied orbital and reaches the vacuum. In the present approach, the vacuum is represented by the virtual orbitals, with the further hypothesis that ionization has the same probability from each of these orbitals, which are the channels via which ionization

occurs. As the dynamics evolves, the flux can bring the electron back to the original orbital, or it can also evolve towards a different occupied orbital, which has become unoccupied in the dynamics. If the orbital is higher in energy, *i.e.*, less binding than the initial orbital, the flux can then reach a higher lying virtual orbital. Energy is conserved in the process, and the apparent simplicity of equation 1 exposed.

Analysis and Discussion

Coronene Ultraviolet Spectrum: Results of the CAM-B3LYP/CCPVDZ calculations for coronene in D6h symmetry, displayed as convoluted spectra in Figure 1(b), are compared in Table 1 with the ADC(3) previous theoretical values by Deleuze *et al.*³⁷, as well as with experimental data. Results of the CAM-B3LYP/CCPVDZ calculations on the statistical ensemble of distorted molecules are displayed in Figure 1(c). In this latter case, it is not possible to assign the irreducible representations of the orbitals, although the energies are not greatly affected by the distortions. Effectively, peaks of both spectra are positioned nearly at the same binding energies, although Figure 1(c) shows further broadened bands, in better agreement with the experimental profile – Figure 1(a). The ultraviolet photoemission spectrum of coronene is characterized by two main regions: the π -ionization system, below 10 eV, with two sharp and well separated bands, labelled as A and B; the broad σ -band system, with four intense and rather sharp peaks (C to F) and a further couple of broad bands, G-H - see Figures 1(b) and 1(c).

Table 1 gives the detailed orbital assignment for all these bands at the D6h geometry. Our calculations place the vertical ionization threshold at 6.77 eV for the “cooled” coronene molecule, in good agreement with the ADC(3) results (6.71 eV)³⁷ and the experimental value by Boschi *et al.* (7.34 eV).¹¹⁶ Analogous calculations (not reported here) at the B3LYP/6-31G* level places the vertical ionization at 5.64 eV, demonstrating how a large basis set incorporating diffuse functions combined with an exchange-correlation functionals with long-range (1/r) corrections is necessary to reproduce peaks positions more accurately. Peaks A and B, in the π region, are both underestimated with respect to the experimental bands, with a shift of about 0.6 eV.

ADC(3) calculations identified three dominant shake-up satellite configurations in this region, namely [s1], [s2] and [s3], placed at 9.33, 10.91 and 11.92 eV, with a corresponding pole strength of 0.026, 0.192 and 0.083. All of them correlate with $2e_{2u}^{-2} 3e_{1g}^{+1}$ state.³⁷ In our spectrum, these shake-up lines overlap with one-electron transitions. Their contribution to the current density probability between e_{2u} and e_{1g} molecular orbitals corresponds to 1.3% of the total band, in agreement with both low pole strength of the ADC(3) results and the low intensity peaks of the experimental spectrum.

In the analysis of the σ -band system, for sake of simplicity, we refer to the constant field strength UPS profile. We identified four intense, well separated peaks, labelled from C to F, at binding energies of

TABLE 1. Results of CAM-B3LYP/CCPVDZ on Coronene (D6h Symmetry Point Group) for the valence photoemission spectrum

Level	MO SYMM	CAM-B3LYP/CCPVDZ	ADC(3) ^b	Experiment
1	E2U	6.771	6.711	7.3-7.6
2	E1G	8.333	8.336	8.6-8.7
3	B2G	8.762	9.332 [s ¹] ^a	
			8.680 <i>a</i>	
			12.147	
4	B1G	8.983	8.808	9.12-9.22
			11.197 [s ³] ^a	
5	A2U	10.276	10.184 ^a	10.3
			10.916 [s ²] ^a	
6	E2G	10.308	10.590	10.55
7	E2U	10.798	10.456 ^a	
8	B2U	11.508	11.931	
9	E1U	11.528	11.988	11.5
10	A2G	11.892	12.491	12.28
11	B1U	11.926	12.468	
12	E1G	12.435	12.330 ^a	
13	E2G	12.744	12.263	13.05
14	B2U	13.179	13.773	13.57
15	E1U	13.282	13.873	
16	A1G	13.481	14.064	
17	A2U	13.690	13.242 ^a	
18	E2G	14.254	14.824	
19	E1U	14.361	14.943	
20	E2G	14.820	15.465 ^a	
21	A1G	16.016	16.727 ^a	
22	B2U	16.590	17.283 ^a	
23	E1U	16.650	17.274 ^a	
24	B1U	17.154	17.833 ^a	
25	A2G	17.295	17.926 ^a	
26	A1G	19.118	<i>a</i>	
27	E1U	19.293		
28	E2G	21.589	<i>a</i>	

^a Breakdown of the molecular orbital picture of ionization. ^b Values from ref. 37.

TABLE 2. Results of CAM-B3LYP/CCPVDZ on Coronene (D6h Symmetry Point Group) for core-level photoemission spectrum. CAM-B3LYP/CCPVDZ energies are scaled by a factor of 1.037

Level	MO SYMM	CAM-B3LYP/CCPVDZ	Literature Calculations ^a	Literature Experiment ^a
1	B1U	279.54*1.037 (289.88)	289.30	289.90
2	E2G	279.54*1.037 (289.88)		
3	E1U	279.54*1.037 (289.88)		
4	E1U	279.52*1.037 (289.86)		
5	E2G	279.52*1.037 (289.86)	289.26	
6	B1U	279.52*1.037 (289.86)		
7	A1G	279.37*1.037 (289.70)		
8	E1U	279.37*1.037 (289.70)	289.02	289.70
9	E2G	279.37*1.037 (289.70)		
10	B1U	279.37*1.037 (289.70)		

^a Values from ref. 38.

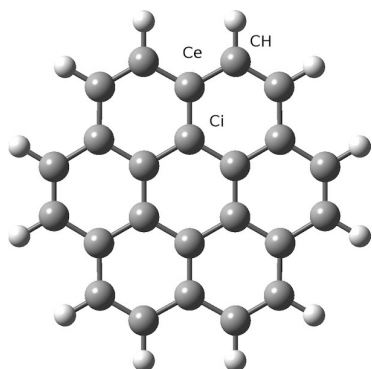


Figure 5. Schematic illustration of coronene with non-equivalent carbon atom labels.

about 10.32, 11.6, 12-13.4 and 14.44 eV, in agreement with experimental data (see Table 1). The peak D obtained with a variable field envelope shows the main discrepancy with the constant field strength spectrum, being located at about 12.5 eV. Bands G and H, not registered in the experimental spectrum, are compared to ADC(3) calculations. The peak G, placed at a binding energy of 16.65 eV by our simulations, is preceded and followed by two shoulders, at binding energies of 16.03 and 17.2 eV, respectively. These results are fully consistent with an intense and asymmetric signal indicated by PIES (Penning Ionization Electron Spectra) measurements by Ohno and co-workers¹¹⁷ and also reported by Deleuze *et al.*³⁷ They are in agreement with ADC(3) results, even if shifted at

lower energy by about 1.0 eV. The higher shoulder is related to shake up lines of the 23 e1u orbital, according to Deleuze *et al.*³⁷ The last peak (H) is the result of a series of shake-up features related to the inner valence orbitals. For these peaks, shake-up lines become evident since their energy position does not overlap with any of the one-electron transitions.

Coronene C1s Spectrum: Results of the CAM-B3LYP/CCPVDZ calculations on the D6h symmetry of coronene are shown as convoluted spectra in Figure 2(b), while those on the statistical ensemble of distorted molecules are displayed in Figure 2(c). In the calculated C1s photoemission spectrum, peaks need to be scaled by a factor of 1.037 for better comparison with the experimental data. The orbital assignment for the core level spectrum of cooled coronene is summarized in Table 2, together with a comparison with previous theoretical and experimental data.³⁸ Two main different peaks can be ascribed to distinct C1s orbitals, namely the core orbitals localized on innermost (Ci) and outer carbons (Ce), at around 289.9 eV – (already scaled value) and core orbitals localized on external carbons bound to hydrogen (CH), at 289.70 eV (already scaled value) - see Figure 5. The calculation of the C1s spectrum for the thermally distorted coronene molecules allows reproducing the shoulder of the experimental profile – see Figure 2(a), characterized by a vibrational progression towards higher BE values.

Conclusions

A simple time-propagation model is able to simulate with reasonable accuracy the valence band and core level photoemission spectra of coronene. The model exposes the rich complexity of transitions that is hidden under the apparent simplicity of the equation that governs photoelectron spectroscopy. Electron fluxes occur from the occupied states to the continuum represented by the unoccupied orbitals. In the dynamics, backscattering to binding orbitals other than the initial one can occur, thereby starting new flows to orbitals that apparently do not match the photon energy. The quantum mechanical nature of the processes makes the sequence outlined above true only for explicative purposes, since all processes occur simultaneously in less than 10 fs. It is important to note that this model is equally suitable for the interpretation of two-photon photoemission, where it could also be applied to explain phenomena like laser assisted photoemission.¹¹⁸ In fact, it may reveals complex correlated electron relaxation processes by describing femtosecond-to-attosecond time-scale electron dynamics in solids and in surface-adsorbate systems. Despite the intricacy of ionization spectra and the extent of the shake-up contamination of the band system, the method provides consistent insights into both valence and core-level photoemission spectra.

Acknowledgements

The measurements at ELETTRA were supported by the "Access to Research Infrastructure" action of the improving Human Potential Program (ARI) of the EU. This work has been supported by MIUR (PRIN 2010-2011, Italy).

References

- K. M. Siegbahn, *Nobel Lecture in Nobel Lectures in physics* (1981-1990), World Scientific Publishing Co. Pte. Ltd, 1993.
- S. Huefner, *Photoelectron Spectroscopy*, Springer-Verlag, Berlin, 2003.
- H. G. Muller, *Phys. Rev. Lett.*, 1999, **83**, 3158.
- M. J. Nandor, M. A. Walker, L. D. Van Woerkom and H. G. Muller, *Phys. Rev. A*, 1999, **60**, R1771.
- H. G. Muller, *Phys. Rev. A*, 1999, **60**, 1341
- M. Thachuk, M. Y. Ivanov, D. M. Wardlaw, *J. Chem. Phys.*, 1998, **109**, 5747.
- M. Thachuk, M. Y. Ivanov, D. M. Wardlaw, *J. Chem. Phys.*, 1996, **105**, 4094.
- K. Harumiya, H. Kono, Y. Fujimura, I. Kawata, A. D. Bandrauk, *Phys. Rev. A*, 2002, **66**, 43403.
- T. D. G. Walsh, F. A. Ilkov, S. L. Chin, F. Chateauueuf, T. T. Nguyen-Dang, S. Chelkowski, A. D. Bandrauk, O. Atabek, *Phys. Rev. A*, 1998, **58**, 3922.
- H. T. Yu, T. Zuoand, A. D. Bandrauk, *Phys. Rev. A*, 1996, **54**, 3290.
- A. Talebpour, K. Vijayalakshmi, A. D. Bandrauk, T. T. Nguyen-Dang, S. L. Chin, *Phys. Rev. A*, 2000, **62**, 42708.
- M. Lein, T. Kreibich, E. K. U. Gross, V. Engel, *Phys. Rev. A*, 2002, **65**, 033403.
- I. Kawata, A. D. Bandrauk, H. Kono, Y. Fujimura, *Laser Phys.*, 2001, **11**, 188.
- A. D. Bandrauk, H. Z. Lu, *Phys. Rev. A*, 2000, **62**, 53406.
- A. D. Bandrauk, S. Chelkowski, J. Levesque, *Laser Phys.*, 2002, **12**, 468.
- A. D. Bandrauk, S. Chelkowski, *Phys. Rev. Lett.*, 2000, **84**, 3562.
- S. Chelkowski, M. Zamojski, A. D. Bandrauk, *Phys. Rev. A*, 2001, **63**, 23409.
- H. T. Yu, A. D. Bandrauk, V. Sonnad, *J. Math. Chem.*, 1994, **15**, 287.
- T. Zuo, A. D. Bandrauk, *Phys. Rev. A*, 1995, **51**, R26.
- L. Tao, C. W. McCurdy, T. N. Rescigno, *Phys. Rev. A*, 2009, **79**, 012719.
- M. Brosolo, P. Decleva, *Chem. Phys.*, 1992, **159**, 185.
- M. Brosolo, P. Decleva, A. Lisini, *J. Phys. B*, 1992, **25**, 3345.
- M. Brosolo, P. Decleva, A. Lisini, *Comput. Phys. Commun.*, 1992, **71**, 207.
- A. Leger, L. D'hendecourt, N. Boccarra, *Polycyclic Aromatic Hydrocarbons and Astrophysics*, Eds. Dordrecht, The Netherlands, 1987.
- H. Andrews, C. Boersma, M. W. Werner, J. Livingston, L. J. Allamandola, A. G. M. Tielens, *Astrophys. J.*, 2015, **807**, 99; A. M. Cook, A. Ricca, A. L. Mattioda, J. Bouwman, J. Roser, H. Linnartz, J. Bregman, L. J. Allamandola, *Astrophys. J.*, 2015, **799**, 14; S. H. Cuyllé, L. J. Allamandola, H. Linnartz, *Astron. Astrophys.*, 2014, **562**, A22; C. Boersma, J. Bregman, L. J. Allamandola, *Astrophys. J.*, 2013, **769**, 117; F. Salama, P. Ehrenfreund, in *The Diffuse Interstellar Bands, Proceedings of the International Astronomical Union 9, Symposium 297*, eds. Cami, J., Cox, N. (Cambridge Journals Online), 2013, 364.
- M. Wagner, U. Bolm-Audorff, J. Hegewald, A. Fishta, P. Schlattmann, J. Schmitt, A. Seidler, *Occup. Environ. Med.*, 2015, **72**, 226.
- M. Vojtisek-Lom, M. Pechout, L. Dittrich, V. Beranek, M. Kotek, J. Schwarz, P. Vodicka, A. Milcova, A. Rossnerova, A. Ambroz, J. Topinka, *Atmos. Environ.*, 2015, **109**, 9.
- S. Verlaak, S. Steudel, P. Heremans, D. Janssen, M. Deleuze, *Phys. Rev. B*, 2003, **68**, 195409.
- S. Veerlak, V. Arkhipov, P. Heremans, *App. Phys. Lett.*, 2003, **82**, 75; F. R. Baptista, S. A. Belhout, S. Giordani, S. S. J. Quinn, *Chem. Soc. Rev.*, 2015, **44**, 4433.
- J. Schirmer, L. S. Cederbaum, O. Walter, *Phys. Rev. A*, 1983, **28**, 1237; W. von Niessen, J. Schirmer, L. S. Cederbaum, *Comput. Phys. Rep.*, 1984, **1**, 57; J. Schirmer, G. Angonoa, *J. Chem. Phys.*, 1989, **91**, 1754.
- L. S. Cederbaum, M. Domcke, *Adv. Chem. Phys.*, 1977, **36**, 205.
- Y. Ohrn, G. Born, *Adv. Quantum Chem.*, 1981, **13**, 1; J. V. Ortiz, *The Electron Propagator Picture of Molecular Electronic Structure; Computational Chemistry: Reviews of Current Trends*, ed Leszczynski, J. (World Scientific: Singapore), 1997; Vol. 2, p 1.
- J. Schirmer, *J. Phys. Rev. A*, 1991, **43**, 4647; F. Mertins, J. Schirmer, *Phys. Rev. A*, 1996, **53**, 2153.
- M. S. Deleuze, *Int. J. Quantum Chem.*, 2003, **93**, 191.
- M. S. Deleuze, M. K. Scheller, L. S. Cederbaum, *J. Chem. Phys.*, 1995, **103**, 3578.
- A. Golod, M. S. Deleuze, L. S. Cederbaum, *J. Chem. Phys.*, 1999, **110**, 6014.
- M. S. Deleuze, *J. Phys. Chem. A*, 2004, **108**, 9244.
- G. Fronzoni, O. Baseggio, M. Stener, H. Weijie, T. Guangjun, Y. Luo, B. Apicella, M. Alfè, M. de Simone, A. Kivimaki, M. Coreno, *J. Chem. Phys.*, 2014, **141**, 044313.
- Z. L. Cai, K. Sendt, J. R. Reimers, *J. Chem. Phys.*, 2002, **117**, 5543; J. R. Reimers, Z.-L. Cai, A. Bilic, A. S. Hush, *Ann. N. Y. Acad. Sci.*, 2003, **110**, 235.
- D. J. Tozer, R. D. Amos, N. C. Handy, B. J. Roos, L. Serrano-Andres, *Mol. Phys.*, 1999, **97**, 859; S. Grimme, M. Parac, *Chem. Phys.*, 2003, **292**, 11; A. L. Sobolowski, W. Domcke, *Chem. Phys.*, 2003, **294**, 73; A. Dreuw, G. R. Fleming, M.

- Head-Gordon, *Phys. Chem. Chem. Phys.*, 2003, **5**, 3247; A. Dreuw, G. R. Fleming, M. Head-Gordon, *J. Phys. Chem. B*, 2003, **107**, 6500.
- 41 A. Dreuw, J. L. Weisman, M. Head-Gordon, *J. Chem. Phys.*, 2003, **119**, 2943.
- 42 A. Dreuw, M. Head-Gordon, *J. Am. Chem. Soc.*, 2004, **126**, 4007.
- 43 G. Wu, P. Hockett, A. Stolow, *Phys. Chem. Chem. Phys.*, 2011, **13**, 18447; J. H. D. Eland, *Photoelectron Spectroscopy*, Butterworths & Co. Publishers, 2nd ed., 1985; K-J. Yuan, S. Chellkoeski, A. D. Bandrauk, *J. Chem. Phys.*, 2013, **138**, 134316.
- 44 O. Plekan, V. Feyer, R. Richter, M. Coreno, M. de Simone, K. C. Prince, V. J. Carravetta, *J. Phys. Chem. A*, 2007, **111**, 10998.
- 45 R. Boschi, W. Schmidt, *Tetrahedron Lett.*, 1972, **25**, 2577.
- 46 R. E. Allen, *Phys. Rev. B*, 1994, **50**, 18629.
- 47 J. S. Graves, R. E. Allen, *Phys. Rev. B*, 1998, **58**, 13627.
- 48 B. R. Torralva, R. E. Allen, *J. Mol. Opt.*, 2002, **49**, 593.
- 49 Y. S. Dou, B. R. Torralva, R. E. Allen, *J. Mod. Opt.*, 2003, **50**, 2615.
- 50 A. Acocella, G. A. Jones, F. Zerbetto, *J. Phys. Chem. Lett.*, 2012, **3**, 3610.
- 51 A. Acocella, F. Carbone, F. Zerbetto, *J. Am. Chem. Soc.*, 2010, **132**, 12166.
- 52 A. Acocella, G. A. Jones, F. Zerbetto, *J. Phys. Chem. B*, 2010, **114**, 4101.
- 53 G. A. Jones, A. Acocella, F. Zerbetto, *J. Phys. Chem. A*, 2008, **112**, 9650.
- 54 G. A. Jones, A. Acocella, F. Zerbetto, *Theor. Chem. Acc.*, 2007, **118**, 99.
- 55 A. Acocella, G. A. Jones, F. Zerbetto, *J. Phys. Chem. A*, 2006, **110**, 5164.
- 56 R.E. Allen, T. Dumitrica, and B. Torralva, *Ultrafast Physical Processes in Semiconductors*, edited by K.T. Tsen Academic, New York, 2001, Chap. 7
- 57 J. Crank, P. Nicolson, *Proc. Camb. Phil. Soc.*, 1947, **43**, 50.
- 58 Z. G. Sun, W. T. Yang, *J. Chem. Phys.*, 2011, **134**, 041101; E. Lorin, A. D. Bandrauk, 2010, *Comp. Phys. Comm.*, **181**, 626
- 59 M. R. Hermann, J. A. Fleck, Jr., *Phys. Rev. A*, 1988, **38**, 6000.
- 60 A. D. Bandrauk, H. Shen, *Chem. Phys. Lett.*, 1991, **176**, 428.
- 61 G. Avila, T. Carrington, Jr., *Quantum Dynamic Imaging*, edited by A. D. Bandrauk and M. Ivanov, Springer, New York, 2011, p. 1.
- 62 L. Y. Peng and A. F. Starace, *J. Chem. Phys.*, 2006, **125**, 154311.
- 63 P. Pillet, C. Drag, B. L. Tolra, *Laser Phys.*, 2001, **11**, 480 and references cited therein
- 64 A. N. Nikolov, J. R. Ensher, E. Eyler, H. Wang, W. C. Stwalley, P. L. Gould, *Phys. Rev. Lett.*, 2000, **84**, 246 and references cited therein.
- 65 A. D. Bandrauk, E. Dehghanian, H. Z. Lu, *Chem. Phys. Lett.*, 2006, **419**, 346.
- 66 Schiff, L. I. *Quantum Mechanics*, 3rd ed.; McGraw-Hill: New York, 1968.
- 67 Levin, I. N. *Quantum Mechanics*, 3rd ed.; Allyn and Bacon: Boston, 1983.
- 68 O. Keller, *Quantum theory of near-field electrodynamics*, Springer, New York, 2011.
- 69 M. Wollenhaupt, V. Engel, T. Baumert, *Annu. Rev. Phys. Chem.*, 2005, **56**, 25–56
- 70 K. Bolton, W. L. Hase, G. H. Peslherbe, *Modern Methods for Multidimensional Dynamics Computation in Chemistry*, ed. D. L. Thompson (World Scientific: Singapore), 1998, 143.
- 71 W. Chen, W. L. Hase, H. B. Schlegel, *Chem. Phys. Lett.*, 1994, **228**, 436; J. M. Millam, V. Bakken, W. Chen, W. L. Hase, H. B. Schlegel, *J. Chem. Phys.*, 1999, **111**, 3800; X. Li, J. M. Millam, H. B. Schlegel, *J. Chem. Phys.*, 2000, **113**, 10062.
- 72 Gaussian 09, Revision D.01, M. J. Frisch, G. W. Trucks, H. B. Schlegel, G. E. Scuseria, M. A. Robb, J. R. Cheeseman, G. Scalmani, V. Barone, B. Mennucci, G. A. Petersson, H. Nakatsuji, M. Caricato, X. Li, H. P. Hratchian, A. F. Izmaylov, J. Bloino, G. Zheng, J. L. Sonnenberg, M. Hada, M. Ehara, K. Toyota, R. Fukuda, J. Hasegawa, M. Ishida, T. Nakajima, Y. Honda, O. Kitao, H. Nakai, T. Vreven, J. A. Montgomery, Jr., J. E. Peralta, F. Ogliaro, M. Bearpark, J. J. Heyd, E. Brothers, K. N. Kudin, V. N. Staroverov, R. Kobayashi, J. Normand, K. Raghavachari, A. Rendell, J. C. Burant, S. S. Iyengar, J. Tomasi, M. Cossi, N. Rega, J. M. Millam, M. Klene, J. E. Knox, J. B. Cross, V. Bakken, C. Adamo, J. Jaramillo, R. Gomperts, R. E. Stratmann, O. Yazyev, A. J. Austin, R. Cammi, C. Pomelli, J. W. Ochterski, R. L. Martin, K. Morokuma, V. G. Zakrzewski, G. A. Voth, P. Salvador, J. J. Dannenberg, S. Dapprich, A. D. Daniels, Ö. Farkas, J. B. Foresman, J. V. Ortiz, J. Cioslowski, and D. J. Fox, Gaussian, Inc., Wallingford CT, 2009.
- 73 C. S. Sloane, W. L. Hase, *J. Chem. Phys.*, 1977, **66**, 1523.
- 74 T. Helgaker, E. Uggerud, H. J. A. Jensen, *Chem. Phys. Lett.*, 1990, **173**, 145.
- 75 E. Uggerud, T. Helgaker, *J. Am. Chem. Soc.*, 1992, **114**, 4265.
- 76 J. P. Perdew, R.G. Parr, M. Levy, J. L. Balduz, *Phys. Rev. Lett.*, 1982, **49**, 1691–1694.
- 77 M. Levy, J. Perdew, V. Sahni, *Phys. Rev. A*, 1984, **30**, 2745–2748.
- 78 C.-O. Almbladh, U. von Barth, *Phys. Rev. B*, 1985, **31**, 3231–3244.
- 79 J. Perdew, M. Levy, *Phys. Rev. B*, 1997, **56**, 16021–16028.
- 80 S. Kummel, L. Kronik, *Rev. Mod. Phys.*, 2008, **80**, 3.
- 81 E. J. Baerends, P. Ros, *Chem. Phys.*, 1973, **2**, 52–59
- 82 J. P. Perdew, *Chem. Phys. Lett.*, 1979, **64**, 127–130.
- 83 U. Salzner, R. Baer, *J. Chem. Phys.*, 2009, **131**, 231101.
- 84 C. Faber, C. Attaccalite, V. Olevano, E. Runge, X. Blase, *Phys. Rev. B*, 2011, **83**, 115123.
- 85 A. M. Teale, F. De Proft, D. J. Tozer, *J. Chem. Phys.*, 2008, **129**, 044110.
- 86 L. Kronik, T. Stein, S. Refaely-Abramson, R. Baer, *J. Chem. Theory Comput.*, 2012, **8**, 1515–1531.
- 87 R. M. Martin, *Electronic Structure: Basic Theory and Practical Methods*; Cambridge University Press: Cambridge, U. K., 2004
- 88 T. Leininger, H. Stoll, H.-J. Werner, A. Savin, *Chem. Phys. Lett.*, 1997, **275**, 151–160.
- 89 T. Yanai, D. P. Tew and N. C. Handy, *Chem. Phys. Lett.*, 2004, **393**, 51.
- 90 H. Ikura, T. Tsuneda, T. Yanai and K. Hirao, *J. Chem. Phys.*, 2001, **115**, 3540.
- 91 Y. Tawada, T. Tsuneda, S. Yanagisawa, T. Yanai, K. Hirao, *J. Chem. Phys.*, 2004, **120**, 8425.
- 92 A. Savin, *Recent Developments and Applications of Modern Density Functional Theory*, ed. J. M. Seminario, Elsevier, Amsterdam, 1996.
- 93 M. Kamiya, T. Tsuneda, K. Hirao, *J. Chem. Phys.*, 2002, **117**, 6010.
- 94 J. Heyd, G. E. Scuseria, M. Ernzerhof, *J. Chem. Phys.*, 2003, **118**, 8207.
- 95 J. Toulouse, F. Colonna, A. Savin, *Phys. Rev. A*, 2004, **70**, 062505.
- 96 R. Baer, D. Neuhauser, *Phys. Rev. Lett.*, 2005, **94**, 043002.
- 97 T. Yanai, R. J. Harrison, N. C. Handy, *Mol. Phys.*, 2005, **103**, 413
- 98 R. Baer, E. Livshits, U. Salzner, *Annu. Rev. Phys. Chem.*, 2010, **61**, 85–109
- 99 N. Mardirossian, M. Head-Gordon, *J. Chem. Phys.*, 2014, **140**, 18A527
- 100 C.R. Zhang, J.S. Sears, B. Yang, S.G. Aziz, V. Coropceanu, J. L. Bredas, *J. Chem. Theory Comput.*, 2014, **10**, 2379.

- 101 D. Jacquemin, C. Adamo, *J. Chem. Theory Comput.*, 2011, **7**, 369.
- 102 T. Korzdorfer, J. S. Sears, C. Sutton, J. L. Bredas, *J. Chem. Phys.*, 2011, **135**, 204107
- 103 O. Svoboda, M. Oncák, P. Slavíček, *The Journal of Chem Phys*, 2011, **135**, 154302.
- 104 B. Kovač, I. Ljubić, A. Kivimäki, M. Coreno, I. Novak, *Phys. Chem. Chem. Phys.*, 2015, **17**, 10656–10667
- 105 R. van Leeuwen, E. J. Baerends, *Phys. Rev. A*, 1994, **49**, 2421.
- 106 T. H. Dunning Jr., *J. Chem. Phys.*, 1989, **90**, 1007.
- 107 X. Lee, S. M. Smith, A.N. Markevitch, D.A. Romanov, R. J. Levis, H. B. Schlegel, *Phys. Chem. Chem. Phys.*, 2005, **7**, 233.
- 108 V. Keldysh, *Sov. Phys. JETP*, 1965, **20**, 1307
- 109 M. J. DeWitt and R. J. Levis, *Phys. Rev. Lett.*, 1998, **81**, 5101.
- 110 S. M. Smith, X. S. Li, A. N. Markevitch, D. A. Romanov, R. J. Levis, H. B. Schlegel, *J. Phys. Chem. A*, 2005, **109**, 10527.
- 111 S. M. Smith, X. S. Li, A. N. Markevitch, D. A. Romanov, R. J. Levis, H. B. Schlegel, *J. Phys. Chem. A*, 2005, **109**, 5176.
- 112 S. M. Smith, X. S. Li, A. Markevitch, D. Romanov, R.J. Levis, H.B. Schlegel, *J. Phys. Chem. A*, 2007, **111**, 6920.
- 113 S. M. Hankin, D. M. Villeneuve, P. B. Corkum, D. M. Rayner, *Phys. Rev. A*, 2001, **64**, 013405,.
- 114 S. M. Hankin, D. M. Villeneuve, P. B. Corkum, D. M. Rayner, *Phys. Rev. Lett*, 2000, **84**, 5082.
- 115 M. Lezius, V. Blanchet, M. Yu Ivanov, A. Stolow, *J. Chem. Phys.*, 2002, **117**, 1575.
- 116 R. Boschi, J. N. Murrel, W. Schmidt, *Discuss. Faraday, Soc.*, 1972, **54**, 116.
- 117 H. Yanakado, Y. Sawada, H. Shinohara, K. Ohno, *J. Electron Spectrosc. Relat. Phenom.*, 1998, **927**, 88.
- 118 L. Miaja-Avila, C. Lei, M. Aeschlimann, J. L. Gland, M. M. Murnane, H. C. Kapteyn, G. Saathoff, *Phys. Rev. Lett.*, 2006, **97**, 113604; L. Miaja-Avila, G. Saathoff, S. Mathias, J. Yin, C. La-o-vorakiat, M. Bauer, M. Aeschlimann, M. M. Murnane, H. C. Kapteyn, *Phys. Rev. Lett.* 2008, **101**, 046101.